International Journal of Solids and Structures 50 (2013) 680–686

Contents lists available at SciVerse ScienceDirect

International Journal of Solids and Structures

journal homepage: www.elsevier.com/locate/ijsolstr

Electrostatically tunable band gaps in finitely extensible dielectric elastomer fiber composites

Gal Shmuel *

Division of Engineering and Applied Science, California Institute of Technology, Pasadena, CA 91125, United States

ARTICLE INFO

Article history:
Received 8 August 2012
Received in revised form 24 October 2012
Available online 12 November 2012

Keywords:
Dielectric elastomers
Wave propagation
Band-gap
Phononic crystal
Plane-wave expansion method
Finite deformations

ABSTRACT

The structure of band-gaps in actuated fiber-reinforced dielectric elastomer composites with square lattice is studied. The constitutive behaviors of the phases are characterized by an augmented Gent strain energy density function, to account for the strain-hardening of the elastomer. The finite static deformation of the composite is calculated when subjected to an electric bias field along the fibers. The anti-plane mode of small electroelastic waves propagating in the material deformed configuration is determined by means of a proper adjustment of the plane-wave expansion method. The resultant eigenvalue problem supplies the dispersion relation from which bands of prohibited frequencies are determined.

The band structures of exemplary composites with circular fibers are evaluated for various values of the bias electric field. The dependency on the properties and volume fractions of the phases, and most importantly the bias electric field is explored. It is revealed how enhancing the intensity of the electrostatic field widens the bands and shifts them toward higher frequencies. These results suggest the use of dielectric elastomer composites as control mechanisms for electroelastic wave propagation by properly tuning the electrostatic excitation.

1. Introduction

Wave propagation in periodic elastic composites, also known as *phononic crystals* (Kushwaha et al., 1993), received much attention in the last decades, e.g., the works of Sigalas and Economou (1992), Kushwaha et al. (1994), Tanaka and Tamura (1998) and Gei et al. (2004), to name a few. The interest is mainly in virtue of the fascinating *band gaps* (BGs) phenomenon observed in these structures (Kushwaha et al., 1994). The appearance of these ranges of frequencies at which elastic waves cannot propagate enables applications such as isolators, noise suppressors, filters, and more. The interest has been extended to periodic piezoelectric structures (Hou et al., 2004; Qian et al., 2008a; Wang et al., 2009, 2010; Hu et al., 2012), in pursuit of improving their implementations in transducers, sensors and medical ultrasonic imaging, to name a few.

A novel family of soft smart materials known as *dielectric elastomers* (DEs) (Pelrine et al., 2000a), offers a new transmission medium for both electric and elastic waves (Dorfmann and Ogden, 2010). The motivation for using DEs stems from their ability to sustain strains of more than 200% (Pelrine et al., 2000b) and having their mechanical and electrical properties modified in response to an electric stimulation. This offers an almost unexplored potential for manipulating electroelastic waves by tuning the applied bias fields. To the best of the author's knowledge, this type of control mechanism was first proposed by Gei et al. (2011) who considered small flexural wave propagation along a periodically piecewise actuated DE plate, though considering only the elastic fields and governing equations of the perturbed problem. Later on Shmuel et al. (2012) investigated the propagation of incremental electroelastic waves in an actuated layer by solving the coupled electric and elastic equations, showing how the propagation velocity strongly depends on the electric excitation.

These results led Shmuel et al. (2012) to use DEs as the constituents of an electrostatically actuated periodic laminate subjected to incremental shear motions. The evaluation of the pertinent band structure demonstrated how by controlling the electrostatic bias field desired frequencies can be filtered out. Continuing along this path, in this paper the study is extended to a two-dimensional system by investigating the band structure for the anti-plane mode of electroelastic waves propagating in finitely strained circular fiber-reinforced composites with square lattice. As the forthcoming results demonstrate, *undesired frequencies can be actively filtered out by properly tuning the bias electric field*.

The paper is composed in the following manner. Following the works of Dorfmann and Ogden (2005), deBotton et al. (2007), Suo et al. (2008), Dorfmann and Ogden (2010), Tian et al. (2012), Castañeda et al. (2012) and Shmuel et al. (2012), Section 2 revisits the required dynamical theory of DE composites. The response of DE composites with square arrays of fibers of arbitrary cross-section

* Tel.: +1 626 395 3629; fax: +1 626 568 2719.
E-mail address: galshm@caltech.edu

0020-7683/$ - see front matter © 2012 Elsevier Ltd. All rights reserved.
http://dx.doi.org/10.1016/j.ijsolstr.2012.10.028

to an electric field along the fibers is calculated in Section 3. The behaviors of the composite phases are assumed to be governed by the *incompressible dielectric Gent model* (DG). The Gent model (Gent, 1996) composing the elastic part of the augmented strain energy density function was derived in aim to capture the strain-stiffening observed in polymers (Arruda and Boyce, 1993). The anti-plane motion of incremental electroelastic waves superimposed on the deformed configuration of the composite is determined next. To this end, a proper extension of the plane-wave expansion (PWE) method (Kushwaha et al., 1993) to the case of finitely deformed DE composites is formulated. A numerical study of the band structure is performed in Section 4 for an exemplary properties of a composite with circular fibers to investigate the dependency on the phases properties and volume fractions. Most importantly, the variation of the band diagram as function of the bias electric field is demonstrated. The main conclusions and observations are summarized in Section 5.

2. Dynamics of dielectric elastomer composites

Let $\Omega_0 \subset \mathbb{R}^3$ denote the volume region of a heterogeneous body made out of N perfectly bonded different homogeneous electroelastic phases, with $\partial\Omega_0$ being the external boundary of the body with the surrounding vacuum. The volume region $\Omega_0^{(r)}$ $(r = 1, 2, \ldots, N)$ of each phase has its boundary $\partial\Omega_0^{(r)}$. The mapping of a material point $\mathbf{X}$ from the reference configuration of the body to a point $\mathbf{x}$ in its current configuration Ω with boundary $\partial\Omega$ is $\boldsymbol{\chi} : \Omega_0 \times \mathscr{I} \to \mathbb{R}^3$, $\mathbf{x} = \boldsymbol{\chi}(\mathbf{X}, t)$, and assumed to be continuous and twice-differentiable. The notation of $\mathbf{v} = \boldsymbol{\chi}_{,t}$, $\mathbf{a} = \boldsymbol{\chi}_{,tt}$ and $\mathbf{F} = \nabla_{\mathbf{X}}\boldsymbol{\chi} \equiv \frac{\partial \boldsymbol{\chi}}{\partial \mathbf{X}}$ for the corresponding velocity, acceleration, and deformation gradient is employed, respectively. Let $\mathrm{d}\mathbf{X}$, $\mathrm{d}A$, $\mathrm{d}V$ and ρ_L denote the referential line, area, volume elements and mass density in the neighborhood of $\mathbf{X}$, respectively. These are transformed to their deformed counterparts via $\mathrm{d}\mathbf{x} = \mathbf{F}\mathrm{d}\mathbf{X}$, $\mathbf{N}\mathrm{d}A = \frac{1}{J}\mathbf{F}^{\mathrm{T}}\mathbf{n}\mathrm{d}a$, $\mathrm{d}v = J\mathrm{d}V$ and $\rho = \rho_L/J$, where $J \equiv \det(\mathbf{F}) > 0$, $\mathbf{N}$ is the unit normal to the referential area element, and $\mathbf{n}$ is its counterpart in the current configuration. The right and left Cauchy-Green strain tensors are $\mathbf{C} = \mathbf{F}^{\mathrm{T}}\mathbf{F}$ and $\mathbf{b} = \mathbf{F}\mathbf{F}^{\mathrm{T}}$, respectively.

The electric field $\mathbf{e}$ in the deformed configuration is commonly derived as the gradient of a scalar electrostatic potential field. The relation between the electric displacement field $\mathbf{d}$ and $\mathbf{e}$ in free space is $\mathbf{d}^\star = \epsilon_0\mathbf{e}^\star$, where ϵ_0 is vacuum permittivity. Herein and in the sequel a star superscript notation denotes fields outside the material. In dielectric bodies an adequate constitutive relation is required.

The equations of motion are

$$\nabla \cdot \boldsymbol{\sigma} = \rho\mathbf{a}, \tag{1}$$

where $\boldsymbol{\sigma}$ is the 'total' stress tensor (Dorfmann and Ogden, 2005), symmetric on account of the balance of angular momentum, and consisting of both mechanical and electrical contributions. The total stress relates the traction $\mathbf{t}$ to a deformed area element with a unit normal $\mathbf{n}$ by

$$\boldsymbol{\sigma}\mathbf{n} = \mathbf{t}. \tag{2}$$

For the ideal dielectrics (no free body charge), and by considering a quasi-electrostatic approximation, the electric governing equations read

$$\nabla \cdot \mathbf{d} = 0, \quad \nabla \times \mathbf{e} = \mathbf{0}, \tag{3}$$

for Gauss law and Faraday law, respectively. The Maxwell stress $\boldsymbol{\sigma}^\star$ outside the body is given in terms of the outer electric field $\mathbf{e}^\star$

$$\boldsymbol{\sigma}^\star = \epsilon_0\left[\mathbf{e}^\star \otimes \mathbf{e}^\star - \frac{1}{2}(\mathbf{e}^\star \cdot \mathbf{e}^\star)\mathbf{I}\right], \tag{4}$$

where $\mathbf{I}$ is the identity tensor. The following jump conditions take place across the outer boundary

$$(\boldsymbol{\sigma} - \boldsymbol{\sigma}^\star)\mathbf{n} = \mathbf{t}_m, \quad (\mathbf{e} - \mathbf{e}^\star) \times \mathbf{n} = \mathbf{0}, \quad \left(\mathbf{d} - \mathbf{d}^\star\right) \cdot \mathbf{n} = -w_e, \tag{5}$$

where w_e is the surface charge density, and $\mathbf{t}_m$ is a prescribed mechanical traction. The traction $\mathbf{t}$ is postulated as a sum of the prescribed mechanical traction $\mathbf{t}_m$ and an electric traction $\mathbf{t}_e$ resulting from the Maxwell stress, such that $\mathbf{t}_e = \boldsymbol{\sigma}^\star\mathbf{n}$. Across an internal charge-free boundary between two phases m and f the jump conditions read

$$[\![\boldsymbol{\sigma}]\!]\mathbf{n} = \mathbf{0}, \quad [\![\mathbf{d}]\!] \cdot \mathbf{n} = 0, \quad [\![\mathbf{e}]\!] \times \mathbf{n} = \mathbf{0}, \tag{6}$$

where $[\![\bullet]\!] \equiv (\bullet)^{(m)} - (\bullet)^{(f)}$ denotes the jump of fields between the two phases.

The 'total' first Piola–Kirchhoff stress, Lagrangian electric displacement and electric field, respectively, are

$$\mathbf{P} = J\boldsymbol{\sigma}\mathbf{F}^{-\mathrm{T}}, \quad \mathbf{D} = J\mathbf{F}^{-1}\mathbf{d}, \quad \mathbf{E} = \mathbf{F}^{\mathrm{T}}\mathbf{e}, \tag{7}$$

satisfying the Lagrangian form of the governing Eqs. (1) and (3)

$$\nabla_{\mathbf{X}} \cdot \mathbf{P} = \rho_L\mathbf{a}, \quad \nabla_{\mathbf{X}} \cdot \mathbf{D} = 0, \quad \nabla_{\mathbf{X}} \times \mathbf{E} = \mathbf{0}, \tag{8}$$

with the referential jump conditions across $\partial\Omega_0$

$$(\mathbf{P} - \mathbf{P}^\star)\mathbf{N} = \mathbf{t}_M, \quad (\mathbf{D} - \mathbf{D}^\star) \cdot \mathbf{N} = -w_E, \quad (\mathbf{E} - \mathbf{E}^\star) \times \mathbf{N} = \mathbf{0}, \tag{9}$$

where $\mathbf{t}_M\mathrm{d}A = \mathbf{t}_m\mathrm{d}a$ and $w_E\mathrm{d}A = w_e\mathrm{d}a$. Eq. (6) transforms to

$$[\![\mathbf{P}]\!]\mathbf{N} = \mathbf{0}, \quad [\![\mathbf{D}]\!] \cdot \mathbf{N} = 0, \quad [\![\mathbf{E}]\!] \times \mathbf{N} = \mathbf{0}. \tag{10}$$

Adopting the formulation of Dorfmann and Ogden (2005), the total first Piola–Kirchhoff stress and the Lagrangian electric field are derived from an *augmented energy density function* Ψ, with the independent variables $\mathbf{F}$ and $\mathbf{D}$, such that

$$\mathbf{P} = \frac{\partial\Psi}{\partial\mathbf{F}}, \quad \mathbf{E} = \frac{\partial\Psi}{\partial\mathbf{D}}. \tag{11}$$

For incompressible materials the kinematic constraint suggests the use of a Lagrange multiplier p_0, such that the first of (11) obtains the form

$$\mathbf{P} = \frac{\partial\Psi}{\partial\mathbf{F}} - p_0\mathbf{F}^{-\mathrm{T}}. \tag{12}$$

Note that p_0 can only be determined from the boundary conditions together with the equations of motion.

Following Dorfmann and Ogden (2010), an infinitesimal time-dependent elastic and electric displacements $\dot{\mathbf{x}} = \dot{\boldsymbol{\chi}}(\mathbf{X}, t)$ and $\dot{\mathbf{D}}(\mathbf{X}, t)$ are superimposed next on the static deformed configuration $\Omega(\boldsymbol{\chi})$. Henceforth superposed dot is employed to denote incremental quantities. The *push-forwards* of increments in the total first Piola–Kirchhoff stress, the Lagrangian electric displacement and electric fields, respectively, are

$$\boldsymbol{\Sigma} = \frac{1}{J}\dot{\mathbf{P}}\mathbf{F}^T, \quad \check{\mathbf{d}} = \frac{1}{J}\mathbf{F}\dot{\mathbf{D}}, \quad \check{\mathbf{e}} = \mathbf{F}^{-T}\dot{\mathbf{E}}, \tag{13}$$

and satisfy the incremental governing equations

$$\nabla \cdot \boldsymbol{\Sigma} = \rho\dot{\mathbf{x}}_{,tt}, \quad \nabla \cdot \check{\mathbf{d}} = 0, \quad \nabla \times \check{\mathbf{e}} = \mathbf{0}. \tag{14}$$

The incremental kinematic constraint of incompressible materials is

$$\mathrm{tr}(\mathbf{h}) = 0, \tag{15}$$

where $\mathbf{h} = \nabla\dot{\mathbf{x}}$ is the displacement gradient. When linearizing in the increments, the following incremental constitutive relations are derived

$$\boldsymbol{\Sigma} = \mathscr{C}\mathbf{h} + p_0\mathbf{h}^{\mathrm{T}} - \dot{p}_0\mathbf{I} + \mathscr{B}\check{\mathbf{d}}, \tag{16}$$

$$\check{\mathbf{e}} = \mathscr{B}^{\mathrm{T}}\mathbf{h} + \mathscr{A}\check{\mathbf{d}}, \tag{17}$$

where $(\mathscr{B}^{\mathrm{T}}\mathbf{h})_k = \mathscr{B}_{ijk}h_{ij}$. The constitutive tensors $\mathscr{A}$, $\mathscr{B}$ and $\mathscr{C}$ are the push-forwards of the referential reciprocal dielectric tensor $\mathscr{A}_0$, electroelastic coupling tensor $\mathscr{B}_0$, and elasticity tensor $\mathscr{C}_0$

$$\mathscr{A}_{0\alpha\beta}=\frac{\partial^2\Psi}{\partial D_\alpha\partial D_\beta},\quad \mathscr{B}_{0i\alpha\beta}=\frac{\partial^2\Psi}{\partial F_{i\alpha}\partial D_\beta},\quad \mathscr{C}_{0i\alpha k\beta}=\frac{\partial^2\Psi}{\partial F_{i\alpha}\partial F_{k\beta}},\tag{18}$$

such that

$$\mathscr{A}_{ij}=JF^{-1}_{\alpha i}\mathscr{A}_{0\alpha\beta}F^{-1}_{\beta j},\quad \mathscr{B}_{ijk}=F_{j\alpha}\mathscr{B}_{0i\alpha\beta}F^{-1}_{\beta k},\quad \mathscr{C}_{ijkl}=\frac{1}{J}F_{j\alpha}\mathscr{C}_{0i\alpha k\beta}F_{l\beta}.\tag{19}$$

3. Anti-plane motion of finitely deformed DE fiber composites

Consider an infinite periodic lattice of square arrays of length A in the (x_1,x_3) plane. The arrays are composed of infinitely long DE fibers along the x_2 direction with arbitrary cross-section embedded in a different DE matrix (Fig. 1a). In the sequel quantities associated with the fiber phase are denoted with a superscript f, and quantities associated with the matrix phase are denoted with a superscript m.

The phases behaviors are characterized by the DG model

$$\Psi^{(p)}_{DG}(I_1,I_{5e})=-\frac{\mu^{(p)}J^{(p)}_m}{2}\ln\left(1-\frac{I_1-3}{J^{(p)}_m}\right)+\frac{1}{2\epsilon^{(p)}}I_{5e},\quad p=m,f,\tag{20}$$

where $I_1=\mathrm{tr}(\mathbf{C})$, $I_{5e}=\mathbf{D}\cdot\mathbf{CD}$, $\mu^{(p)}$ denote the phases shear moduli, and $\epsilon^{(p)}=\epsilon_0\epsilon^{(p)}_r$ denote the dielectric constants, with $\epsilon^{(p)}_r$ being the phases relative dielectric constant. The dimensionless locking parameter J_m (Gent, 1996) corresponds to the strain-stiffening exhibited in elastomers. This *lock-up effect* is a result of the finite extensibility of the polymer chains. Making use of Eq. (11), the total stress evolving in each phase is

$$\boldsymbol{\sigma}^{(p)}=\frac{\mu^{(p)}}{1-\frac{I_1^{(p)}-3}{J^{(p)}_m}}\mathbf{b}^{(p)}+\frac{1}{\epsilon^{(p)}}\mathbf{d}^{(p)}\otimes\mathbf{d}^{(p)}-p^{(p)}_0\mathbf{I},\tag{21}$$

where the electric displacement field is related to the electric field via

$$\mathbf{d}^{(p)}=\epsilon^{(p)}\mathbf{e}^{(p)}.\tag{22}$$

The composite is assumed to be free of prescribed mechanical tractions, while an electric field e_2 is applied in the x_2 direction along the fibers. From a practical viewpoint, the actuation is executed by applying a voltage drop between two compliant coated electrodes on the top and bottom faces at 'infinity'.

In each phase the following uni-modular (on account of incompressibility) diagonal deformation gradients are assumed

$$[\mathrm{F}]^{(p)}=\mathrm{diag}\left[\lambda^{(p)}_1,(\lambda^{(p)}_1\lambda^{(p)}_3)^{-1},\lambda^{(p)}_3\right].\tag{23}$$

The perfect bonding between the phases dictates that the stretch ratios in the matrix and the fibers are identical in the x_2 direction, i.e.,

$$\left(\lambda^{(m)}_1\lambda^{(m)}_3\right)^{-1}=\left(\lambda^{(f)}_1\lambda^{(f)}_3\right)^{-1}.\tag{24}$$

In virtue of the symmetry of the problem in the x_1-x_3 plane the pertinent stretch ratios within each phase are same

$$\lambda^{(p)}_1=\lambda^{(p)}_3.\tag{25}$$

Utilizing Eq. (23) together with Eqs. (24) and (25) implies that the resultant configuration of each phase agrees with the homogeneous deformation gradient

$$[\mathrm{F}]^{(m)}=[\mathrm{F}]^{(f)}=\mathrm{diag}\left[\lambda,\lambda^{-2},\lambda\right].\tag{26}$$

When specialized to the considered problem, the in-plane stress components emanating from Eq. (21) are

$$\begin{aligned}\sigma^{(p)}_{11}&=\sigma^{(p)}_{33}=\mu^{(p)}\frac{\lambda^2}{1-\frac{2\lambda^2+\lambda^{-4}-3}{J^{(p)}_m}}-p^{(p)}_0,\\ \sigma^{(p)}_{22}&=\mu^{(p)}\frac{\lambda^{-4}}{1-\frac{2\lambda^2+\lambda^{-4}-3}{J^{(p)}_m}}+\epsilon^{(p)}e_2^2-p^{(p)}_0,\end{aligned}\tag{27}$$

where $e^{(m)}_2=e^{(f)}_2=e_2$. The fact that the composite is free to expand in the (x_1,x_3) plane yields

$$\sigma^{(p)}_{11}=\sigma^{(p)}_{33}=0,\tag{28}$$

leading to the following expression for the pressure of each phase

$$p^{(p)}_0=\mu^{(p)}\frac{\lambda^2}{1-\frac{2\lambda^2+\lambda^{-4}-3}{J^{(p)}_m}}.\tag{29}$$

The remaining boundary condition in the x_2 direction translates to

$$v^{(m)}\sigma^{(m)}_{22}+v^{(f)}\sigma^{(f)}_{22}=0,\tag{30}$$

where $v^{(m)}$ and $v^{(f)}=1-v^{(m)}$ are the volume fractions of the matrix and fiber phase, respectively. Eq. (29) together with Eq. (30) yields a relation between the resultant in-plane stretch ratio λ, and the applied electric field. Assuming $J^{(m)}_m=J^{(f)}_m\equiv J_B$, the relation can be written in a simple implicit form

$$\frac{\lambda^2-\lambda^{-4}}{1-\frac{2\lambda^2+\lambda^{-4}-3}{J_B}}=\frac{\bar{\epsilon}}{\bar{\mu}}e_2^2,\tag{31}$$

where $(\bar{\bullet})=v^{(f)}(\bullet)^{(f)}+v^{(m)}(\bullet)^{(m)}$

When specialized to the DG model (20) and deformation gradients (26), the components of $\mathscr{A}^{(p)},\mathscr{B}^{(p)}$ and $\mathscr{C}^{(p)}$ are

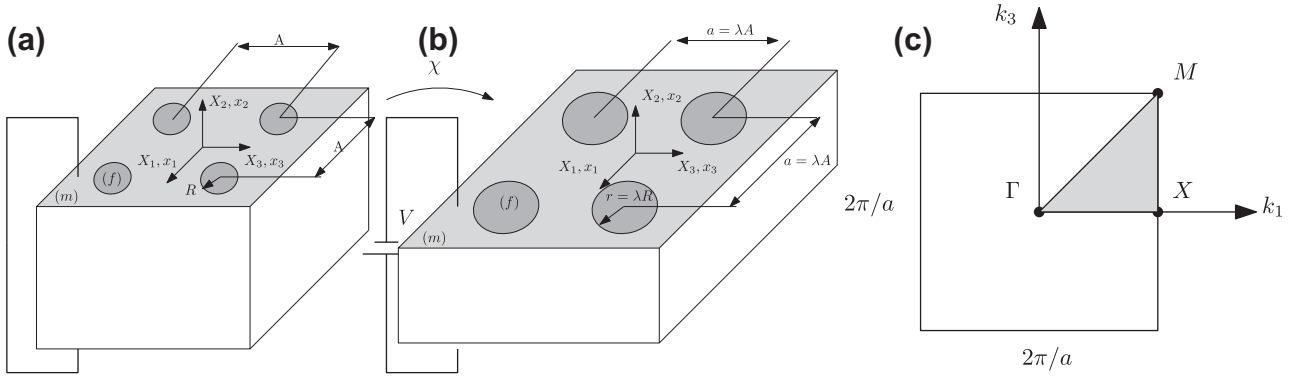

Fig. 1. Square lattice fiber-reinforced composite (a) in the reference configuration and (b) in the deformed configuration, subjected to an electric field parallel to the fibers. (c) The corresponding first irreducible Brillouin zone.

$$\mathscr{A}^{(p)}_{11} = \mathscr{A}^{(p)}_{22} = \mathscr{A}^{(p)}_{33} = \frac{1}{\epsilon^{(p)}}, \tag{32}$$

$$\mathscr{B}^{(p)}_{121} = \mathscr{B}^{(p)}_{211} = \mathscr{B}^{(p)}_{323} = \mathscr{B}^{(p)}_{233} = \frac{1}{2}\mathscr{B}^{(p)}_{222} = e_2, \tag{33}$$

$$\mathscr{C}^{(p)}_{1111} = \mathscr{C}^{(p)}_{2121} = \mathscr{C}^{(p)}_{2323} = \mathscr{C}^{(p)}_{1313} = \mathscr{C}^{(p)}_{3333} = \mu^{(p)}\frac{\lambda^2}{1-\frac{2\lambda^2+\lambda^{-4}-3}{J^{(p)}_m}}, \tag{34}$$

$$\mathscr{C}^{(p)}_{1212} = \mathscr{C}^{(p)}_{2222} = \mathscr{C}^{(p)}_{3232} = \mu^{(p)}\frac{\lambda^{-4}}{1-\frac{2\lambda^2+\lambda^{-4}-3}{J^{(p)}_m}} + \epsilon^{(p)}e_2^2, \tag{35}$$

The propagation in the (x_1, x_3) plane of electroelastic waves superimposed on the aforementioned finite deformation is addressed next. I restrict attention to the anti-plane mode, in which the elastic displacements are in the x_2 direction. Let $\dot{x}_2(x_1, x_3, t)$ and $\varphi(x_1, x_3, t)$ denote, respectively, the incremental displacement and the incremental electric potential, such that $\check{\mathbf{e}}(x_1, x_3, t) = -\nabla\varphi(x_1, x_3, t)$. These fields are to satisfy the incremental equations of motion (14a) along with Gauss Eq. (14b) and and the incompressibility constraint (15). The resulting non-trivial equations are

$$\Sigma_{21,1}(\mathbf{x}, t) + \Sigma_{23,3}(\mathbf{x}, t) = \rho(\mathbf{x})\dot{x}_{2,tt}, \tag{36}$$

$$\check{d}_{1,1}(\mathbf{x}, t) + \check{d}_{3,3}(\mathbf{x}, t) = 0, \tag{37}$$

where it is understood that the spatial dependency is only via the x_1 and x_3 components, in view of the symmetry of the problem in the x_2 direction. In terms of $\dot{x}_2(x_1, x_3, t)$ and $\varphi(x_1, x_3, t)$, Eqs. (36) and (37) are put in the form

$$\nabla_{\mathrm{T}} \cdot (\tilde{\mu}(\mathbf{x})\nabla_{\mathrm{T}}\dot{x}_2 - d_2(\mathbf{x})\nabla_{\mathrm{T}}\varphi) = \rho(\mathbf{x})\dot{x}_{2,tt}, \tag{38}$$

$$\nabla_{\mathrm{T}} \cdot (-d_2(\mathbf{x})\nabla_{\mathrm{T}}\dot{x}_2 - \epsilon(\mathbf{x})\nabla_{\mathrm{T}}\varphi) = 0, \tag{39}$$

where $\tilde{\mu}(\mathbf{x}) = \mu(x_1, x_3)\frac{\lambda^2}{1-\frac{2\lambda^2+\lambda^{-4}-3}{Jm(x_1x_3)}} - \epsilon(x_1, x_3)e_2^2, \nabla_{\mathrm{T}}(\bullet) = \mathbf{i}_1(\bullet)_{,1} + \mathbf{i}_3(\bullet)_{,3}$ is the in-plane gradient operator, and $\mathbf{i}_1$ and $\mathbf{i}_3$ are unit vectors in the x_1 and x_3 directions, respectively. To solve Eqs. (38) and (39), a proper extension of the PWE method (Kushwaha et al., 1994) is employed. The quantities $\tilde{\mu}$, d_2, ϵ and ρ are expanded in two-dimensional Fourier series in virtue of their in-plane periodicity, such that

$$\zeta(\mathbf{x}) = \sum_{\mathbf{G}} \zeta(\mathbf{G}) \exp(i\mathbf{G} \cdot \mathbf{x}), \quad \zeta = \tilde{\mu}, d_2, \epsilon, \rho, \tag{40}$$

where $\{\zeta(\mathbf{G})\}$ are the Fourier coefficients, and the summation is carried over the infinite two-dimensional reciprocal lattice vectors $\{\mathbf{G}\}$. Since the considered Bravais lattice is square of period $a = \lambda A$, its reciprocal lattice is also square with the reciprocal lattice vectors $\mathbf{G} = G_1\mathbf{i}_1 + G_3\mathbf{i}_3 = \frac{2\pi}{a}n_1\mathbf{i}_1 + \frac{2\pi}{a}n_3\mathbf{i}_3$, where n_1 and n_3 are integers. The Fourier coefficients are given by the inversion of the Fourier transform

$$\zeta(\mathbf{G}) = \frac{1}{a^2}\int\int_{a_{cell}} \zeta(\mathbf{x}) \exp(-i\mathbf{G} \cdot \mathbf{x}) \mathrm{d}a, \tag{41}$$

where a_{cell} is the area of the unit cell. Eq. (41) can be written in terms of the average and difference of the quantities $\zeta^{(f)}$ and $\zeta^{(m)}$ as (Kushwaha et al., 1993)

$$\zeta(\mathbf{G}) = \begin{cases} \zeta^{(f)}v^{(f)} + (1 - v^{(f)})\zeta^{(m)} \equiv \bar{\zeta}, & \mathbf{G} = \mathbf{0}, \\ \left(\zeta^{(f)} - \zeta^{(m)}\right)F(\mathbf{G}) \equiv \Delta\zeta F(\mathbf{G}), & \mathbf{G} \neq \mathbf{0}, \end{cases} \tag{42}$$

$$F(\mathbf{G}) = \frac{1}{a^2}\int\int_{a^{(f)}} \exp(-i\mathbf{G} \cdot \mathbf{x}) \mathrm{d}a, \tag{43}$$

where $a^{(f)}$ is the area of the fiber phase.

According to the Bloch theorem (Kittel, 2005), the incremental displacement and the incremental electric potential fields must satisfy

$$\dot{x}_2(\mathbf{x}, t) = \sum_{\mathbf{G}} \dot{x}_2(\mathbf{G}) \exp[i(\mathbf{G} + \mathbf{k}) \cdot \mathbf{x} - i\omega t], \tag{44}$$

$$\varphi(\mathbf{x}, t) = \sum_{\mathbf{G}} \varphi(\mathbf{G}) \exp[i(\mathbf{G} + \mathbf{k}) \cdot \mathbf{x} - i\omega t], \tag{45}$$

where ω is the angular frequency, and $\mathbf{k} = k_1\mathbf{i}_1 + k_3\mathbf{i}_3$ is the Bloch wave vector restricted to the irreducible first Brillouin zone representing the smallest region where wave propagation is unique. Substitution of Eqs. (42), (44) and (45) in Eqs. (36) and (37) yields

$$\begin{aligned} &\sum_{\mathbf{G},\mathbf{G}'} \left(\tilde{\mu}(\mathbf{G})\dot{x}_2(\mathbf{G}') - d_2(\mathbf{G})\varphi(\mathbf{G}')\right)(\mathbf{G} + \mathbf{G}' + \mathbf{k}) \\ &\quad \cdot (\mathbf{G}' + \mathbf{k}) \exp\left[i(\mathbf{G} + \mathbf{G}' + \mathbf{k}) \cdot \mathbf{x} - i\omega t\right] \\ &\quad = \omega^2 \sum_{\mathbf{G},\mathbf{G}'} \rho(\mathbf{G})\dot{x}_2(\mathbf{G}') \exp\left[i(\mathbf{G} + \mathbf{G}' + \mathbf{k}) \cdot \mathbf{x} - i\omega t\right], \end{aligned} \tag{46}$$

$$\begin{aligned} &\sum_{\mathbf{G},\mathbf{G}'} \left(-d_2(\mathbf{G})\dot{x}_2(\mathbf{G}') - \epsilon(\mathbf{G})\varphi(\mathbf{G}')\right)(\mathbf{G} + \mathbf{G}' + \mathbf{k}) \\ &\quad \cdot (\mathbf{G}' + \mathbf{k}) \exp\left[i(\mathbf{G} + \mathbf{G}' + \mathbf{k}) \cdot \mathbf{x} - i\omega t\right] = 0. \end{aligned} \tag{47}$$

Eqs. (46) and (47) are multiplied by $\exp(-i\mathbf{G}'' \cdot \mathbf{x})$, and integrated over the unit-cell. As a consequence of the orthogonality property of Fourier series only terms satisfying $\mathbf{G} + \mathbf{G}' + \mathbf{k} = \mathbf{G}''$ do not vanish. Thus, we remain with only summation over $\mathbf{G}'$ in the form

$$\begin{aligned} &\sum_{\mathbf{G}'} \left(\tilde{\mu}(\mathbf{G} - \mathbf{G}')\dot{x}_2(\mathbf{G}') - d_2(\mathbf{G} - \mathbf{G}')\varphi(\mathbf{G}')\right)(\mathbf{G} + \mathbf{k}) \cdot (\mathbf{G}' + \mathbf{k}) \\ &\quad = \omega^2 \sum_{\mathbf{G}'} \rho(\mathbf{G} - \mathbf{G}')\dot{x}_2(\mathbf{G}'), \end{aligned} \tag{48}$$

$$\sum_{\mathbf{G}'} \left(-d_2(\mathbf{G} - \mathbf{G}')\dot{x}_2(\mathbf{G}') - \epsilon(\mathbf{G} - \mathbf{G}')\varphi(\mathbf{G}')\right)(\mathbf{G} + \mathbf{k}) \cdot (\mathbf{G}' + \mathbf{k}) = 0. \tag{49}$$

A truncation to a finite number of plane waves N is carried out for implementational purposes. In the sequel I set $N = 169$, which corresponds to the values $-6 \leqslant n_1, n_3 \leqslant 6$. In matrix notation one can write

$$\begin{pmatrix} Q^{(1,1)} Q^{(1,2)} \\ Q^{(2,1)} Q^{(2,2)} \end{pmatrix} \begin{bmatrix} \dot{x}_2(\mathbf{G}') \\ \varphi(\mathbf{G}') \end{bmatrix} = \omega^2 \begin{pmatrix} R & 0 \\ 0 & 0 \end{pmatrix} \begin{bmatrix} \dot{x}_2(\mathbf{G}') \\ 0 \end{bmatrix}, \tag{50}$$

where $Q^{(1,1)}$, $Q^{(1,2)}$, $Q^{(2,1)}$, $Q^{(2,2)}$ and R are $N \times N$ matrices given in the appendix. In pursuit of formulating an eigenvalue problem with respect to $\dot{x}_2(\mathbf{G}')$ I employ the relation $\varphi(\mathbf{G}') = -\left(Q^{(2,2)}\right)^{-1} Q^{(2,1)}\dot{x}_2(\mathbf{G}')$, obtainable from Eq. (50). Substitution back and multiplication by R^{-1} from the left yields

$$\widetilde{Q}\dot{x}_2(\mathbf{G}') = \omega^2 R\dot{x}_2(\mathbf{G}'), \tag{51}$$

where $\widetilde{Q} = R^{-1}\left[Q^{(1,1)} - Q^{(1,2)}\left(Q^{(2,2)}\right)^{-1} Q^{(2,1)}\right]$. The band structure is built by solving Eq. (51) for ω as function of the reduced wave vector $\mathbf{k}$ in the periphery of the irreducible first Brillouin zone. As inferred by Kushwaha et al. (1994) and Vasseur et al. (1994), the pertinent BGs extend throughout the whole zone. For the square lattice its periphery is defined by the lines connecting the points $\Gamma = (0, 0)$, $X = (\pi/a, 0)$ and $M = (\pi/a, \pi/a)$, as illustrated in Fig. 1c. I recall that the band structures herein correspond to the anti-plane mode. Accordingly, the emanating BGs are not complete. i.e., they depend in the propagation mode. The study of complete BGs is of major importance and will be considered in future works.

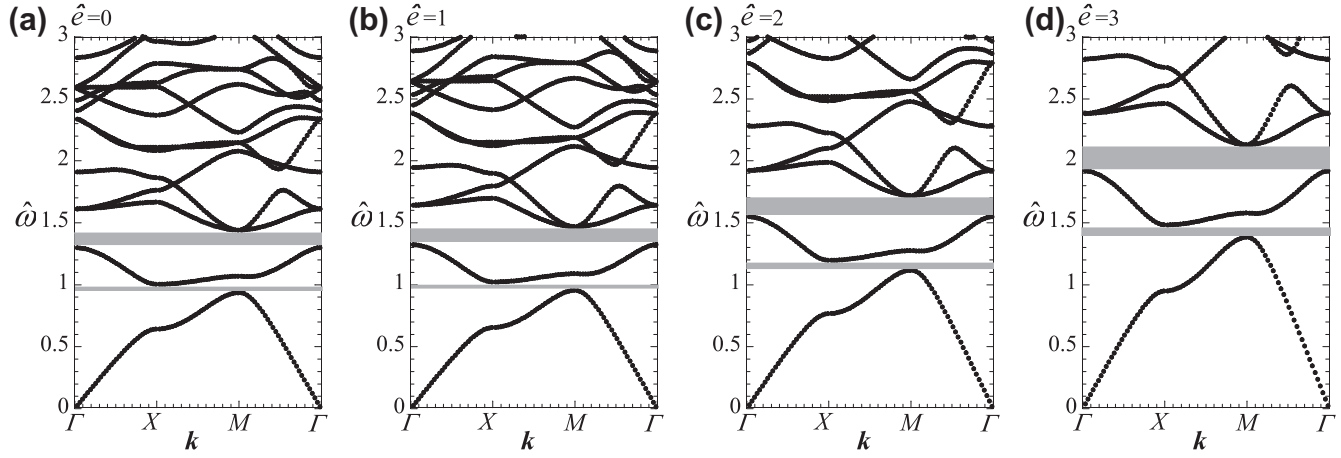

Fig. 2. Band structure of circular fiber-reinforced DG composite subjected to the normalized electric bias fields (a) $\hat{e}=0$, (b) $\hat{e}=1$, (c) $\hat{e}=2$ and (d) $\hat{e}=3$. The normalized frequencies $\hat{\omega}$ are plotted as functions of the reduced wave vector $\mathbf{k}$ along $\Gamma X N \Gamma$. The composite properties are $\rho^{(m)}=\rho^{(f)}=1000\left(\frac{\text{kg}}{\text{m}^3}\right)$, $\mu^{(m)}=2000$ (KPa), $\epsilon_r^{(m)}=3$, and $J_m^{(m)}=J_m^{(f)}=10$ at the values $\alpha=10$, $\beta=10$ and $\nu^{(m)}=0.5$.

4. Numerical investigation of the band structure

The goal is to explore the dependency of the band structure on the properties and volume fractions of the phases, and most importantly on the bias electric field. To this end, I consider an exemplary composite whose matrix properties are

$$\rho^{(m)}=1000\left(\frac{\text{kg}}{\text{m}^3}\right),\quad \mu^{(m)}=2000\ (\text{KPa}),\quad \epsilon_r^{(m)}=3,\quad J_m^{(m)}=10, \tag{52}$$

and evaluate the band structure for representative values of the volume fractions $\nu^{(p)}$, shear contrast $\alpha=\mu^{(f)}/\mu^{(m)}$, permittivity contrast $\beta=\epsilon_r^{(f)}/\epsilon_r^{(m)}$, and the electric bias field e_2. In all of the following examples I assume that $\rho^{(f)}=\rho^{(m)}$ and $J_m^{(f)}=J_m^{(m)}$. Note that $J_m=10$ corresponds to a maximal uniaxial stretch ratio of 3.5. In what follows I find it convenient to use the normalized quantities $c^{(m)}=\sqrt{\mu^{(m)}/\rho^{(m)}}$ and $\hat{\omega}=\omega A/2\pi c^{(m)}$, where $c^{(m)}=\sqrt{\mu^{(m)}/\rho^{(m)}}$. Further, I restrict attention to fibers with circular section of referential radius R, for which the structure function $F(\mathbf{G})$ equals

$$F(\mathbf{G})=2\nu^{(f)}\frac{J_1(Gr)}{Gr},\quad \nu^{(f)}=\frac{\pi r^2}{a^2}, \tag{53}$$

where $r=\lambda R$, and J_1 is the Bessel function of the first kind of order 1.

The main result is demonstrated in Fig. 2, which shows the normalized frequencies $\hat{\omega}$ as functions of the reduced wave vector $\mathbf{k}$ along $\Gamma X M \Gamma$ when the composite is subjected to various normalized electric bias fields $\hat{e}$ at the fixed values $\alpha=10$, $\beta=10$ and $\nu^{(m)}=0.5$. Figs. 2a–d correspond to the normalized bias electric fields $\hat{e}=0$, 1, 2 and 3, respectively. These values result, respectively, in the in-plane stretch ratios $\lambda=1$, 1.2, 1.71 and 2.04. The gray regions in the plots indicate the first and second BGs appearing. The effect of the bias electric field is evident: *as $\hat{e}$ is enhanced, the BGs are shifted toward higher frequency range and their widths are enlarged*. For instance, at the reference configuration, i.e., $\hat{e}=0$, the widths of the first and second BGs are $\Delta\hat{\omega}=0.068$ and 0.141, having their medians at $\hat{\omega}=0.97$ and 1.367, respectively. When the composite is subjected to the normalized electric bias field $\hat{e}=3$, the width of the first and second BGs increase to $\Delta\hat{\omega}=0.1$ and 0.21, with medians at $\hat{\omega}=1.43$ and 2.03, respectively. Thus, by electrostatically actuating the composite the widths of the first and second BGs are increased by a factor of 1.47. The medians are shifted by a similar factor.

Fig. 3 shows the widths of first (continuous curves) and second (dashed curves) BGs as functions of the contrast of the phases properties and volume fractions when applying a normalized electric bias field $\hat{e}=2$. Fig. 3a displays the widths as functions of the shear contrast α at the fixed values of the permittivity contrast $\beta=10$ and matrix volume fraction $\nu^{(m)}=0.5$. Fig. 3b displays the widths as functions of the permittivity contrast β at the fixed values of the shear contrast $\alpha=10$ and matrix volume fraction $\nu^{(m)}=0.5$. It is observed how when the contrasts are enhanced, the widths are enlarged monotonically. The shear contrast plays a more significant role in enlargement of the bands. Fig. 3c displays the widths as functions of the matrix volume fraction $\nu^{(m)}$ at the fixed values of the shear and permittivity contrast $\alpha=\beta=10$. The first gap opens at $\nu^{(m)}=0.4$, reaches a maximum at the vicinity of $\nu^{(m)}=0.45$, and closes at $\nu^{(m)}=0.7$. The second gap undergoes a

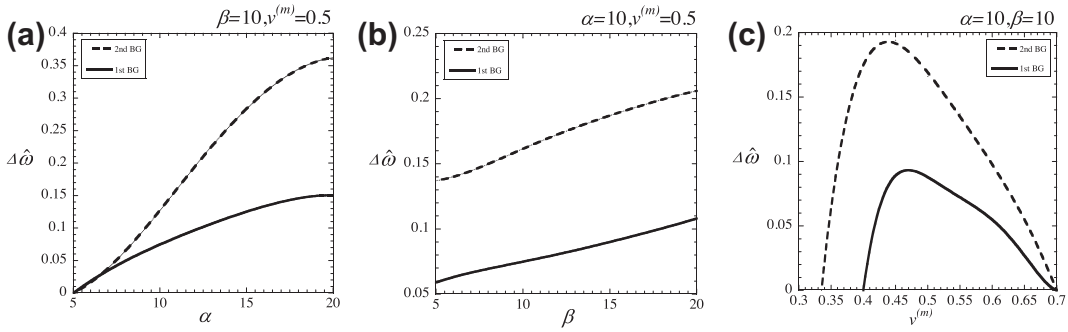

Fig. 3. Widths of first (continuous curves) and second (dashed curves) BGs of circular fiber-reinforced DG composite subjected to a normalized electric bias field $\hat{e}=2$, at the values $\rho^{(m)}=\rho^{(f)}=1000\left(\frac{\text{kg}}{\text{m}^3}\right)$, $\mu^{(m)}=2000$ (KPa), $\epsilon_r^{(m)}=3$, and $J_m^{(m)}=J_m^{(f)}=10$ as functions of (a) the shear contrast α, (b) the permittivity contrast β, and (c) the matrix volume fraction $\nu^{(m)}$.

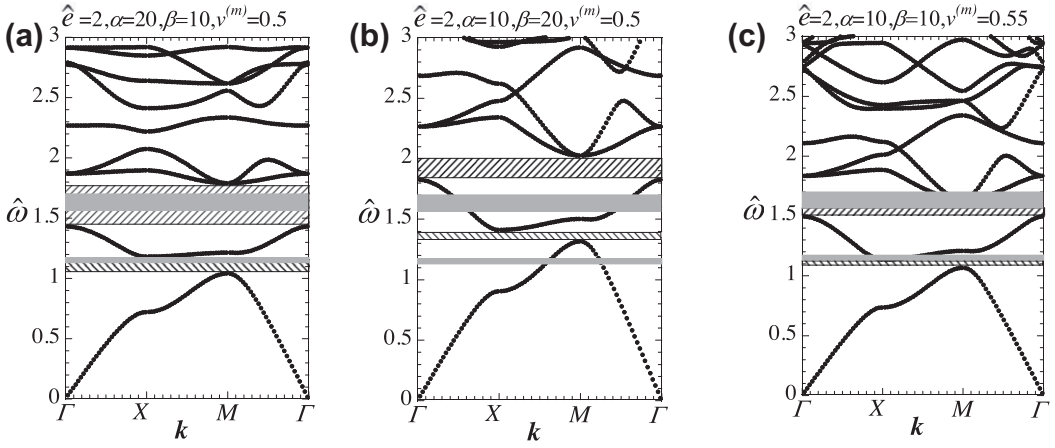

Fig. 4. Band structure of circular fiber-reinforced DG composite subjected to the normalized electric bias field $\hat{e} = 2$, for $\rho^{(m)} = \rho^{(f)} 1000 \left(\frac{\text{kg}}{\text{m}^3}\right)$, $\mu^{(m)} = 2000$ (KPa), $\epsilon_r^{(m)} = 3$, and $J_m^{(m)} = J_m^{(f)} = 10$ at the values (a) $\alpha = 10,\ \beta = 20,\ v^{(m)} = 0.5$ (b) $\alpha = 20, \beta = 10, v^{(m)} = 0.5$, and (c) $\alpha = \beta = 10,\ v^{(m)} = 0.55$. The normalized frequencies $\hat{\omega}$ are plotted as functions of the reduced wave vector $\mathbf{k}$ along $\Gamma X N \Gamma$. The regions of the first and second pertinent BGs are indicated by diagonal lines, where the the gray regions correspond to the first and second BGs associated with a composite characterized by $\alpha = \beta = 10$ and $v^{(m)} = 0.5$ (Fig. 2c).

similar trend, though it opens at a smaller concentration of the matrix volume fraction, namely $v^{(m)} = 0.335$. These trends are in reminiscent of Qian et al. (2008b) observations in the context of piezoelectric phononic crystals. Fig. 4 displays the normalized frequencies $\hat{\omega}$ as functions of the reduced wave vector $\mathbf{k}$ along $\Gamma X M \Gamma$ for exemplary values of α, β and $v^{(m)}$ to illustrate how their variations shifts the bands, when the composite is subjected to $\hat{e} = 2$. Values of $\alpha = 20,\ \beta = 10$ and $v^{(m)} = 0.5$ are chosen in Fig. 4a, $\alpha = 10,\ \beta = 20$ and $v^{(m)} = 0.5$ in Fig. 4b, and $\alpha = \beta = 10$ and $v^{(m)} = 0.55$ in Fig. 4c. The regions of the first and second pertinent BGs are indicated by diagonal lines. For comparison, the gray regions correspond to the first and second BGs associated with a composite characterized by $\alpha = \beta = 10$ and $v^{(m)} = 0.5$ (Fig. 2c). It is observed how increasing the shear contrast in Fig. 4a shifts the bands toward lower frequencies. Conversely, when the permittivity contrast is increased in Fig. 4b the bands are shifted toward higher frequencies. When the concentration of the matrix phase is increased the gaps are moved toward lower frequencies.

5. Concluding remarks

In pursuit of active waveguides/isolators, the band structure of square lattice DE composites with circular fibers is studied, in virtue of the practical importance of this geometry. In particular, the feasibility of controlling these BGs by means of a suitable electrostatic excitation of the composite is examined.

Toward this end, the deformed configuration of a DE matrix reinforced with DE fibers of arbitrary cross-section is determined when applying an electric field parallel to the fibers. The constitutive behaviors of the phases are assumed to be governed by the incompressible dielectric Gent model, oriented to capture the strain-stiffening in polymers. The instantaneous electromechanical properties of the phases are calculated in terms of the bias electric field and resultant in-plane stretch ratio.

The anti-plane mode of small electroelastic waves propagating on top of the finite static deformation is addressed next. To treat the mathematical difficulty stemming from the structure heterogeneity and the coupling between the electric and elastic fields, a proper adjustment of the plane-wave expansion method is formulated. The end result is given in terms of a standard eigenvalue problem for the incremental elastic displacement, from which the dispersion relation is obtained.

Numerical investigation of the band structure is conducted for exemplary composites with circular fibers and various values of the bias electric field. It is showed how increasing the shear and permittivity contrasts results in wider bands. The influence of the matrix volume fraction is explored, revealing how the first and second BGs are maximal when the concentration of the matrix is a bit less than the fibers. Most importantly, evaluation of the frequency spectrum demonstrates how *enhancing the intensity of the bias electric field widens the bands as well as shifts them toward higher frequencies*. These findings suggest the use of DE composites as control mechanisms for electroelastic wave propagation.

Acknowledgments

I am grateful to Prof. G. deBotton for his comments on this work. I also wish to thank Prof. M. Mond for helpful discussions.

Appendix A

The components of the matrices $Q^{(1,1)},\ Q^{(1,2)},\ Q^{(2,1)},\ Q^{(2,2)}$ and R are

$$Q^{(1,1)}_{\mathbf{G},\mathbf{G}'} = \tilde{\mu}(\mathbf{G}-\mathbf{G}')(\mathbf{G}+\mathbf{k})\cdot(\mathbf{G}'+\mathbf{k}), \tag{54}$$

$$Q^{(1,2)}_{\mathbf{G},\mathbf{G}'} = -d_2(\mathbf{G}-\mathbf{G}')\mathbf{G}'(\mathbf{G}+\mathbf{k})\cdot(\mathbf{G}'+\mathbf{k}), \tag{55}$$

$$Q^{(2,1)}_{\mathbf{G},\mathbf{G}'} = Q^{(1,2)}_{\mathbf{G},\mathbf{G}'}, \tag{56}$$

$$Q^{(2,2)}_{\mathbf{G},\mathbf{G}'} = -\epsilon(\mathbf{G}-\mathbf{G}')(\mathbf{G}+\mathbf{k})\cdot(\mathbf{G}'+\mathbf{k}), \tag{57}$$

$$R_{\mathbf{G},\mathbf{G}'} = \rho(\mathbf{G}-\mathbf{G}'). \tag{58}$$

References

Arruda, E.M., Boyce, M.C., 1993. A three-dimensional constitutive model for the large stretch behavior of rubber elastic materials. J. Mech. Phys. Solids 41, 389–412.

deBotton, G., Tevet-Deree, L., Socolsky, E.A., 2007. Electroactive heterogeneous polymers: analysis and applications to laminated composites. Mech. Adv. Mater. Struct. 14, 13–22.

Dorfmann, A., Ogden, R.W., 2005. Nonlinear electroelasticity. Acta Mech. 174, 167–183.

Dorfmann, A., Ogden, R.W., 2010. Electroelastic waves in a finitely deformed electroactive material. IMA J. Appl. Math. 75, 603–636.

Gei, M., Bigoni, D., Franceschini, G., 2004. Thermoelastic small-amplitude wave propagation in nonlinear elastic multilayers. Math. Mech. Solids 9, 555–568.

Gei, M., Roccabianca, S., Bacca, M., 2011. Controlling bandgap in electroactive polymer-based structures. IEEE-ASME Trans. Mechatron. 16, 102–107.

Gent, A.N., 1996. A new constitutive relation for rubber. Rubber Chem. Technol. 69, 59–61.

Hou, Z., Wu, F., Liu, Y., 2004. Phononic crystals containing piezoelectric material. Solid State Commun. 130 (11), 745–749.

Hu, L., Liu, L., Bhattacharya, K., 2012. Existence of surface waves and band gaps in periodic heterogeneous half-spaces. J. Elasticity 107, 65–79.

Kittel, C., 2005. Introduction to Solid State Physics. John Wiley & Sons, Inc., Hoboken, NJ.
Kushwaha, M.S., Halevi, P., Dobrzynski, L., Djafari-Rouhani, B., 1993. Acoustic band structure of periodic elastic composites. Phys. Rev. Lett. 71 (13), 2022–2025.
Kushwaha, M.S., Halevi, P., Martínez, G., Dobrzynski, L., Djafari-Rouhani, B., 1994. Theory of acoustic band structure of periodic elastic composites. Phys. Rev. B 49 (4), 2313–2322.
Pelrine, R., Kornbluh, R., Joseph, J., Heydt, R., Pei, Q.B., Chiba, A., 2000a. High-field deformation of elastomeric dielectrics for actuators. Mater. Sci. Eng. 11, 89–100.
Pelrine, R., Kornbluh, R., Pei, Q.B., Joseph, J., 2000b. High-speed electrically actuated elastomers with strain greater than 100%. Science 287, 836–839.
Ponte Castañeda, P., Siboni, M.H., 2012. A finite-strain constitutive theory for electro-active polymer composites via homogenization. Int. J. Non-Linear Mech. 47 (2), 293–306.
Qian, Z., Jin, F., Li, F., Kishimoto, K., 2008a. Complete band gaps in two-dimensional piezoelectric phononic crystals with 1–3 connectivity family. Int. J. Solids Struct. 45 (17), 4748–4755.
Qian, Z., Kishimoto, K., Jin, F., Wang Z., 2008. Study on the existence of band gaps for the transverse mode in 2d piezoelectric phononic crystals from a point view of connectivity. In: Microwave Conference, pp. 603–607.
Shmuel, G., deBotton, G., 2012. Band-gaps in electrostatically controlled dielectric laminates subjected to incremental shear motions. J. Mech. Phys. Solids 60 (11), 1970–1981. http://dx.doi.org/10.1016/j.jmps.2012.05.006.
Shmuel, G., Gei, M., deBotton, G., 2012. The Rayleigh–Lamb wave propagation in dielectric elastomer layers subjected to large deformations. Int. J. Non-Linear Mech. 47 (2), 307–316.
Sigalas, M.M., Economou, E.N., 1992. Elastic and acoustic wave band structure. J. Sound Vib. 158 (2), 377–382.
Suo, Z., Zhao, X., Greene, W.H., 2008. A nonlinear field theory of deformable dielectrics. J. Mech. Phys. Solids 56 (2), 467–486.
Tanaka, Y., Tamura, S., 1998. Surface acoustic waves in two-dimensional periodic elastic structures. Phys. Rev. B 58 (12), 7958–7965.
Tian, L., Tevet-Deree, L., deBotton, G., Bhattacharya, K., 2012. Dielectric elastomer composites. J. Mech. Phys. Solids 60, 181–198.
Vasseur, J.O., Djafari-Rouhani, B., Dobrzynski, L., Kushwaha, M.S., Halevi, P., 1994. Complete acoustic band gaps in periodic fibre reinforced composite materials: the carbon/epoxy composite and some metallic systems. J. Phys. Condens. Matter 6 (42), 8759.
Wang, Y., Li, F., Kishimoto, K., Wang, Y., Huang, W., 2009. Wave band gaps in three-dimensional periodic piezoelectric structures. Mech. Res. Commun., 0093-6413 36 (4), 461–468.
Wang, Y., Li, F., Kishimoto, K., Wang, Y., Huang, W., 2010. Band gaps of elastic waves in three-dimensional piezoelectric phononic crystals with initial stress. Eur. J. Mech. Solids 29 (2), 182–189.